Deviations of cup anemometer rotational speed measurements due to steady state harmonic accelerations of the rotor

Alejandro Martínez, Enrique Vega, Santiago Pindado *, Encarnación Meseguer, Luis García

Instituto Universitario de Microgravedad "Ignacio Da Riva" (IDR/UPM), ETSI Aeronáutica y del Espacio, Universidad Politécnica de Madrid, Pza. del Cardenal Cisneros 3, Madrid 28040, Spain

ABSTRACT

The measurement deviations of cup anemometers are studied by analyzing the rotational speed of the rotor at steady state (constant wind speed). The differences of the measured rotational speed with respect to the averaged one based on complete turns of the rotor are produced by the harmonic terms of the rotational speed. Cup anemometer sampling periods include a certain number of complete turns of the rotor, plus one incomplete turn, the residuals from the harmonic terms integration within that incomplete turn (as part of the averaging process) being responsible for the mentioned deviations. The errors on the rotational speed due to the harmonic terms are studied analytically and then experimentally, with data from more than 500 calibrations performed on commercial anemometers.

© 2016 Published by Elsevier Ltd.

1. Introduction

The cup anemometer, invented in the XIX century by T.R. Robinson, remains today the most popular wind speed sensor, even taking into account the great development carried out on more sophisticated instruments such as the sonic anemometer, the Lidar, and the Sodar [1]. The performances of this instrument have been thoroughly studied since the XIX century (a quite complete review of the literature on this wind sensor can be found in [2]). As a consequence, different sources of error have been identified in relation to cup anemometer wind speed measurements: turbulence [3–6], non-linearity of the sensor performance [7,8], and the sampling method [9]. Additionally, it should be underlined that uncertainties associated to cup anemometer wind speed measurements have been widely studied, as they are relevant for wind turbines performances [10–12]. According to Eecen and De Noord [13], ISO specifies "two types of uncertainties: category A, the magnitude of which can be deduced from measurements, and category B, which are estimated by other means." The second category, B, takes into account uncertainties related to the anemometer calibration process, such as: wind tunnel correction and calibration; pressure transducer sensitivity and signal conditioning gain; ambient temperature transducer; temperature signal conditioning gain and digital conversion; Pitot tube head coefficient; barometer's sensitivity, signal conditioning gain and signal digital conversion; humidity

correction; and statistical uncertainty associated to the mean of wind speed time series. The reported uncertainty levels by these authors at 10 m/s wind speed were 0.26–0.63% (type A) and 0.3–0.7% (type B).

After a review of the available literature, it can be said that not much effort has been carried out to analyze the cup anemometer errors due to sampling. On the contrary, it seems that the errors related to angular speed sampling on other rotating instruments such as tachometers and speed regulators have been quite deeply studied [14–19]. These instruments normally involve a mechanical design that gives several pulses per turn of the shaft. When measuring the angular speed of a shaft, it is possible to count pulses within a period, to measure the time between two consecutive pulses, or combinations of these two methods [16,17,20]. Regarding the sampling process, some authors suggest to establish the sampling period as a function of the pulse output frequency [14], other authors have suggested the detection of the angular speed averaging the measurement during one turn [19].

A difference between cup anemometer output signal generators and industrial tachometers is the number of pulses per turn. Industrial tachometers give normally a quite high number of pulses per turn (from 290 [17], 720 [15], or 1024 [16] pulses, to 25,000 pulses thanks to integral electronic interpolation over the measurements on a 5000-pulse system [18]), whereas the number of pulses given by cup anemometer is much smaller (from 1 to 44 [21]).

Besides, a specific effect related to cup anemometer performance is its non-constant rotational speed, as a result of the 3-cup configuration that produces three accelerations per turn. Even

2 _A. Martínez et al. / Measurement xxx (2016) xxx–xxx_

in an absolute laminar and steady flow, a cup anemometer rotation speed has not a constant value. In Fig. 1, a relative-to-the-average rotation speed, ω/ω_0, is plotted during one turn. This rotation speed corresponds to the signature of a Thies 4.3303 anemometer measured at 8 m/s wind speed [22]. It can be noted in this figure the aforementioned three accelerations. Considering this speed periodic, it can be expressed in terms of a Fourier expansion:

$$\omega(t) = \omega_0 + \sum_{n=1}^{\infty} \omega_n \sin(n\omega_0 t + \varphi_n), \tag{1}$$

the coefficients corresponding to $n = 3$ and its multiples being the most relevant. See in Table 1 the harmonic terms, ω_n/ω_0, corresponding to the Fourier expansion applied to the data from Fig. 1. See also in Fig. 1 the quite exact approximation to the results given by a 6-harmonic term Fourier series.

However, it should be also pointed out that the 44-pulse per turn output signal system of the Thies 4.3303 anemometer has a certain degree of imperfection, that is, there are up to 10% length differences between pulses measured at a strictly constant rotational speed (i.e., up to 10% length differences between the different teeth of the opto-electronic system's rotating wheel) [22]. In Fig. 2, the relative-to-the-average rotation speed, ω/ω_0, based on the signal given by the opto-electronic output system of the anemometer is plotted. This signature needs to be properly corrected to reach the signature of Fig. 1, this correction being done adjusting each pulse of the turn to the exact length of its corresponding tooth of the opto-electronic system's rotating wheel. In Fig. 2, the 6-harmonic and 3-harmonic terms Fourier expansions applied to the signal are also included. The coefficients of the Fourier series expansion of this uncorrected signature are also included in Table 1. Obviously, greater values are obtained as the mechanical differences between the pulses add a noise pattern to the signature that is repeated every turn of the rotor. Nevertheless, the relative importance of the first and third harmonic terms remains in the Fourier expansion related to the uncorrected signature. In addition, it can be observed in Fig. 2 that the 3-harmonic term Fourier expansion reasonably approaches the corrected rotation speed of the anemometer (represented in the figure by the 6-harmonic term Fourier expansion from Fig. 1).

Even with the problems related to the mechanical differences between pulses of the signal generators, this Fourier expansion has been successfully applied to study cup anemometers and detect anomalies on their performance [23–25]. In the present work the Fourier expansion of the measured rotation speed is used
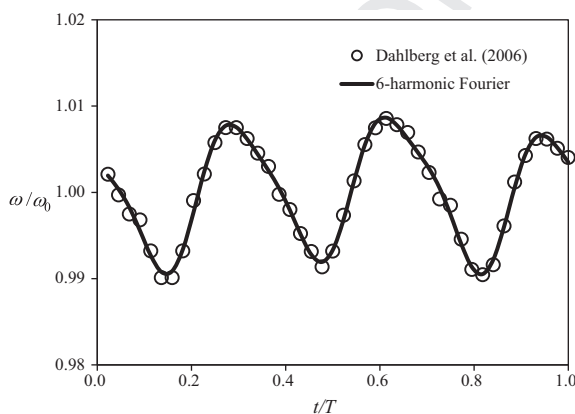
Table 1
Fourier expansion coefficients, i.e., harmonic terms from Eq. (1), related to the corrected and un corrected signatures of a Thies 4.3303 anemometer measured at 8 m/s wind speed [22], see also Figs. 1 and 2.

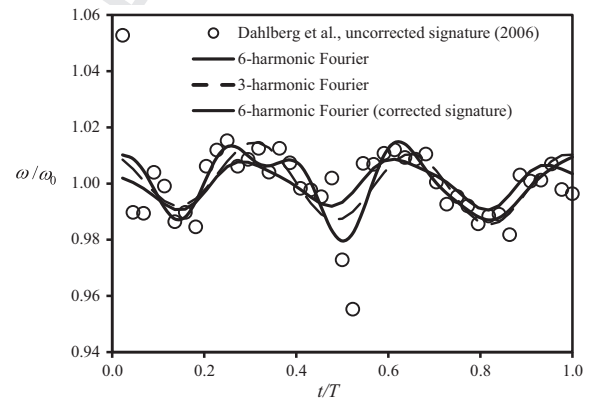| Corrected signature			Uncorrected signature		
n	ω_n/ω_0 (%)	φ_n (°)	n	ω_n/ω_0 (%)	φ_n (°)
1	0.103	−103.92	1	0.310	2.24
2	0.034	−7.76	2	0.152	−47.63
3	0.785	126.14	3	1.187	108.06
4	0.014	28.81	4	0.114	−100.23
5	0.026	−108.88	5	0.468	48.86
6	0.165	−78.58	6	0.326	−85.62
7	0.017	−93.96	7	0.221	37.34
8	0.008	80.81	8	0.102	175.92
9	0.052	121.68	9	0.688	40.28
10	0.011	110.74	10	0.066	3.95
11	0.018	37.31	11	0.585	10.52
12	0.027	8.85	12	0.135	−72.33
13	0.011	−144.03	13	0.428	9.40
14	0.008	−54.78	14	0.358	−67.69
15	0.015	−15.17	15	0.636	−29.79
16	0.013	26.01	16	0.193	−55.31
17	0.010	174.73	17	0.494	−31.54
18	0.016	−134.93	18	0.173	54.57

Fig. 2. Measured cup anemometer's non-dimensional rotational speed, ω/ω_0, along one turn of the rotor. This rotation speed is the uncorrected signature of a Thies 4.3303 anemometer measured at 8 m/s wind speed [22]. The corresponding 6-harmonic and 3-harmonic terms Fourier series expansion has been added to the graph. Also, the 6-harmonic terms Fourier series expansion related to the corrected signature (Fig. 1) is included in the graph.

Fig. 1. Cup anemometer's non-dimensional rotational speed, ω/ω_0, along one turn of the rotor. This rotation speed is the corrected signature of a Thies 4.3303 anemometer measured at 8 m/s wind speed [22] (the uncorrected signature of the anemometer is shown in Fig. 2). The corresponding 6-harmonic terms Fourier series expansion has been added to the graph.

to analyze the effect of the sampling process, which is normally based on fixed periods of time (in general between 1 s and 10 min), programmed on the data-loggers connected to anemometers working on the field.

The aim of the present paper is to study the effect of the sampling period on the mean wind speed measurements, by taking into account the rotor accelerations of the anemometer (i.e., the changes of the rotation speed) along one turn. As the measured wind speed and the rotational frequency are linearly correlated (at normal wind speed ranges, see MEASNET procedures [26]), the present work has been focused on the rotational speed.

2. Cup anemometer's rotation speed sampling period

In Fig. 3 the rotation speed from Fig. 1 has been extrapolated along an hypothetical measurement period, T_d, equal to three rotation periods, T, plus an extra time t' ($t' < T$). Therefore, for a given measurement period, T_d, equal to m rotation periods plus an extra time t', that is, $T_d = mT + t'$, the mean rotation speed can be calculated as:
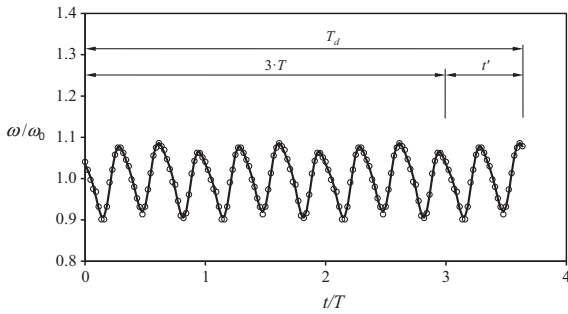
Fig. 3. Example of cup anemometer non-dimensional rotational speed, ω/ω_0, along T_d measurement period that includes 3 turns of the rotor. This graph is based on data from Fig. 1. Open circles stand for the experimental data, whereas the solid line stands for the 6-harmonic approximation of the Fourier expansion (1).

$$\bar{\omega} = \frac{1}{T_d} \int_0^{T_d} \omega(t)\mathrm{d}t = \frac{1}{T_d} \int_0^{T_d} [\omega_0 + \sum_{n=1}^{\infty} \omega_n \sin(n\omega_0 t + \varphi_n)]\mathrm{d}t$$

$$= \omega_0 + \frac{1}{T_d} \int_0^{T_d} \left[\sum_{n=1}^{\infty} \omega_n \sin(n\omega_0 t + \varphi_n) \right]\mathrm{d}t \qquad , \qquad (2)$$

$$= \omega_0 + \frac{1}{mT+t'} \int_0^{t'} \left[\sum_{n=1}^{\infty} \omega_n \sin(n\omega_0 t + \varphi_n) \right]\mathrm{d}t$$

which leads to:

$$\bar{\omega} = \omega_0 + \frac{1}{mT + t'} \sum_{n=1}^{\infty} \frac{1}{n} \frac{\omega_n}{\omega_0} [\cos(\varphi_n) - \cos(n\omega_0 t' + \varphi_n)], \qquad (3)$$

then, if we assume $t' = \eta T$ ($\eta < 1$) and taking into account that $\omega_0 = 2\pi/T$, it is possible to reach the following equation:

$$\bar{\omega} = \omega_0 \left\{ 1 + \frac{1}{2\pi(m+\eta)} \sum_{n=1}^{\infty} \frac{1}{n} \frac{\omega_n}{\omega_0} [\cos(\varphi_n) - \cos(2\pi n\eta + \varphi_n)] \right\}.$$

$$(4)$$

Besides, if the measurement period, T_d, is displaced a time $t^* = -\xi T$ ($\xi < 1$) along the x-axis, and the changes in the Fourier series expansion (1) are taken into account, the above expression can be rewritten as:

$$\bar{\omega} = \omega_0 \left\{ 1 + \frac{1}{2\pi(m+\eta)} \sum_{n=1}^{\infty} \frac{1}{n} \frac{\omega_n}{\omega_0} [\cos(\varphi_n - 2\pi n\xi) \right.$$

$$\left. - \cos(2\pi n\eta + \varphi_n - 2\pi n\xi)] \right\}. \qquad (5)$$

Consequently, the calculated mean speed is composed by two terms, the average rotation speed, ω_0, plus an error which can be expressed by a fraction ε of the rotation speed:

$$\bar{\omega} = \omega_0 + \varepsilon\omega_0 = \omega_0(1+\varepsilon), \qquad (6)$$

Where this relative error ε is defined as:

$$\varepsilon = \sum_{n=1}^{\infty} \varepsilon_n; \varepsilon_n$$

$$= \frac{1}{2\pi(m+\eta)} \frac{1}{n}$$

$$\times \frac{\omega_n}{\omega_0} [\cos(\varphi_n - 2\pi n\xi) - \cos(2\pi n\eta + \varphi_n - 2\pi n\xi)]. \qquad (7)$$

As a result, it can be said that the error ε depends on:

• the number of rotor turns, m, performed in the measurement period, T_d,
• the signature of the rotation, that is, the values of the harmonic terms ω_n/ω_0, and their phase angles, φ_n,

• the extra time, defined by t' or η, besides the m rotor turns, necessary to fulfill the measurement period, T_d,
• and the initial time of the measurement period within the rotational period, defined by ξ.

Nevertheless, it can be assumed that:

$$|\varepsilon_n| \leqslant \varepsilon_n^* = \frac{1}{\pi(m+\eta)} \frac{1}{n} \frac{\omega_n}{\omega_0}. \qquad (8)$$

Therefore, it is possible to define a maximum relative error of the average rotation speed as:

$$\varepsilon^* = \sum_{n=1}^{\infty} \varepsilon_n^* = \sum_{n=1}^{\infty} \frac{1}{\pi(m+\eta)} \frac{1}{n} \frac{\omega_n}{\omega_0}, \qquad (9)$$

bearing in mind, obviously, that this expression represents the upper limit of the calculated error. Furthermore, Eq. (9) can provide some information on which progression of the harmonic terms makes it convergent. For example, if ω_j is the more relevant harmonic term and a progression $\omega_n/\omega_j \sim 1/n$ is assumed, the above equation becomes the well-known Basel problem (solved by Euler in 1974), and then, the following equation can be derived for the maximum relative error:

$$\varepsilon^* \approx \frac{\pi}{6} \frac{1}{(m+\eta)} \left(\frac{\omega_j}{\omega_0} \right). \qquad (10)$$

Taking into account the average calibration constants for the Thies 4.3303 cup anemometer $A = 0.047$ and $B = 0.499$ from [21], which relate the wind speed, V, to the output signal frequency of the anemometer, f:

$$V = A \cdot f + B, \qquad (11)$$

and the number of pulses this sensor gives in one turn, $N_p = 44$, it is possible to derive the period of the turn at $V = 8$ m/s wind speed, $T = 0.2757$ s. In Table 2, the number of turns, m, given by this anemometer in the analyzed sampling periods $T_d = 1, 3, 5, 10$ and 30 s are included, together with the extra time t' necessary to reach the sampling period and the corresponding values of η.

In Fig. 4 the values of error ε calculated in the aforementioned conditions (see Eq. (6)), and for the different sampling periods are shown in relation to the initial time of the measurement period defined by ξ. The maximum values of this error, $\varepsilon_{\max}$, are included in Table 2, together with the maximum error, ε^*, calculated with Eq. (8) (see also Fig. 5). Both the relative errors ε and ε^* were calculated with the 18 harmonic terms included in Table 1 (corrected signature). It can be noted that, as expected, ε^* is larger than the maximum values of ε, both figures being of the same order of magnitude.

The calculation of the maximum error, ε^*, for the selected sampling periods was repeated taking the first three harmonic terms from Table 1 (see Table 2), in order to analyze the relative impact of the harmonic terms from the third one. The results show quite

Table 2
Maximum values of the error in the rotation speed measurements, $\varepsilon_{\max}$, and the maximum error, ε^* (Eq. (8)), performed on an anemometer with the signature from Fig. 1, as a function of the selected sampling periods, T_d. The number of complete turns, m, and additional time, t', contained in these sampling periods have been included in the table. Maximum sampling errors, $\varepsilon_{s,\max}$, calculated for the anemometer with the signature of Fig. 1 (see Section 2.1.), have been also included in the table.

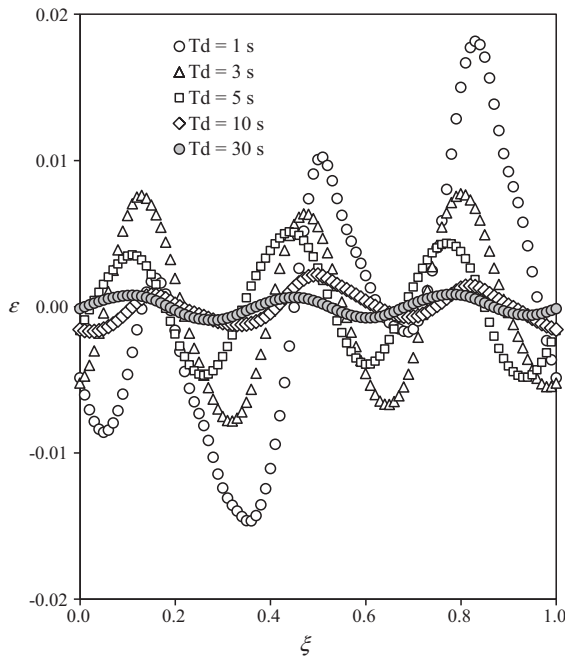| T_d (s)	m	t' (s)	η	$\varepsilon_{\max}$ (%)	ε^* (%)	$\varepsilon_{s,\max}$ (%)
1	3	0.1729	0.627	1.81	3.83	0.372
3	10	0.2430	0.881	0.78	1.28	0.163
5	18	0.03746	0.136	0.51	0.77	0.123
10	36	0.07492	0.272	0.22	0.38	0.0599
30	108	0.2248	0.815	0.09	0.13	0.0183

Fig. 4. Error ε calculated for the different sampling periods, T_d = 1, 3, 5, 10 and 30 s, as a function of the initial time of the measurement period defined by ξ.
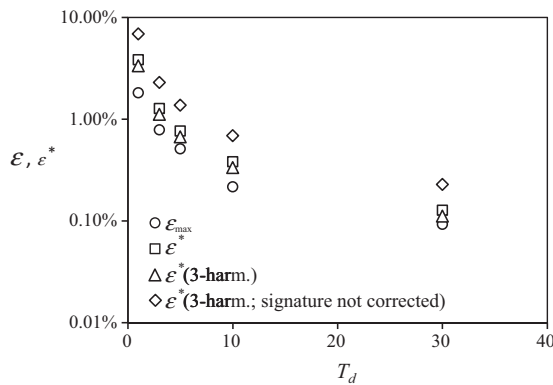

Fig. 5. Maximum values of the error in the rotation speed measurements, ε_{max}, and the maximum calculated error, ε^* (Eq. (8)), performed on an anemometer with the signature from Fig. 1 (ε_{max}, ε^*, ε^*(3-harm.)) and Fig. 2 (ε^*(3-harm.; signature not corrected)) as a function of the selected sampling periods, T_d.

similar figures when compared to the calculations made with the 18 terms from Table 1, see Fig. 5. Therefore, it is possible to say that the contribution to the error due to the sampling period depends mostly on the first three harmonic terms. Finally, the calculations of the maximum error, ε^*, have been performed to the not corrected rotation speed (Fig. 2), taking only the first three harmonic terms from Table 2. These results are also included in Fig. 5. As expected, larger values when compared to the error calculated for the corrected rotation speed are shown. Nevertheless, it should be underlined that the figures are of the same order of magnitude, the trend with the sampling period being also preserved.

2.1. Sampling the anemometer's output signal

The cup anemometer is normally connected to a data-logger when operating in the field. Leaving aside the clock error of the data-logger, the output frequency of the anemometer, f, can be defined as the number of pulses, j, counted in the measurement period, T_d, divided by it. Therefore, this output frequency can be expressed as:

$$f = \frac{j}{T_d} = \frac{mN_p + i}{mT + t'}, \qquad (12)$$

where, as said, m is the number of turns performed by the anemometer's rotor along the measurement period, N_p is the number of pulses per turn given by the anemometer, T, is the rotational period, t' is the extra time required to complete the measurement period once the rotor has completed the m rotations, and i is the number of pulses counted along the extra time t'. From the above equation, the measured rotation speed can be derived as:

$$\bar{\omega} = f\frac{2\pi}{N_p} = \frac{2\pi}{T}\left(\frac{m + \frac{i}{N_p}}{m + \eta}\right) = \omega_0\left(1 + \frac{\frac{i}{N_p} - \eta}{m + \eta}\right). \qquad (13)$$

Therefore, we can obtain the error resulting from a sampling period different from m times the rotational period T:

$$\varepsilon_s = \left|\frac{\frac{i}{N_p} - \eta}{m + \eta}\right|. \qquad (14)$$

Now, the problem is to relate i with η, which can be done calculating the angular displacement, θ, carried out by the rotor in the extra time t':

$$\theta(t') = \int_0^{t'} \omega(t)dt = \int_0^{t'}\left[\omega_0 + \sum_{n=1}^{\infty}\omega_n\sin(n\omega_0 t + \varphi_n)\right]dt, \qquad (15)$$

which leads to:

$$\theta(\eta) = 2\pi\eta + \sum_{n=1}^{\infty}\frac{1}{n}\frac{\omega_n}{\omega_0}[\cos(\varphi_n) - \cos(n\omega_0 t + \varphi_n)]. \qquad (16)$$

Finally, it is possible to derive the number of extra pulses i as the floor of the angular displacement divided by the angular displacement corresponding to one of the pulses, $2\pi/N_p$. Therefore, taking into account an initial phase angle, $2\pi n\xi$, as in Eq. (5), the following equation is obtained:

$$\frac{i}{N_p} = \frac{1}{N_p}\lfloor N_p\{\eta + \frac{1}{2\pi}\sum_{n=1}^{\infty}\frac{1}{n}\frac{\omega_n}{\omega_0}[\cos(\varphi_n - 2\pi n\xi)$$
$$- \cos(2\pi n\eta + \varphi_n - 2\pi n\xi)]\}\rfloor, \qquad (17)$$

which once introduced in expression (14), gives the corresponding error as a function of the harmonic terms of the anemometer output signal.

In Table 2, the maximum errors, $\varepsilon_{s,max}$, (varying ξ from 0 to 1 in steps of 0.01) in relation to the analyzed anemometer (with the signature corrected, see Fig. 1 and Table 1), calculated for the selected sampling periods T_d = 1, 3, 5, 10 and 30 s are included. In these calculations, the 18 terms of the Fourier expansion from Table 1 where used. In order to study the effect of the number of harmonic terms selected, the calculations were repeated taking only the first 3 terms, the results being practically the same. The calculations were also repeated taking the first three harmonic terms corresponding to the uncorrected signature, with no significant changes with respect to the results from Table 2. This fact indicates that the most important term in Eq. (16) is the extra time (defined by η), instead of the harmonic terms produced by the accelerations of the rotor along one turn.

3. Experimental analysis

Data from a large series of calibrations performed to 572 units of two commercial cup anemometers (hereinafter Anemometer-1 and Anemometer-2), was analyzed to study the effect of the

sampling period on cup anemometer measurements from more direct results.

The output signal of these anemometers was sampled at 5 kHz during 20 s at wind speeds V = 4, 7, 10 and 16 m/s during their first calibration (that is, these anemometer were new and not used in the field). The calibrations were performed following MEASNET procedures [27]. More information with regard to the anemometer calibration process carried out at the IDR/UPM calibration facility can be found in [21,28,29].

Firstly, the harmonic terms related to each unit (Eq. (1)), at the selected wind speeds were calculated. This procedure is described in references [23,25]. In Fig. 6, the average value, ω_n/ω_0, and standard deviation, σ, of the first nine harmonic terms calculated in relation to Anemometer-1 and Anemometer-2 units at V = 4 and 16 m/s wind speed are shown. The same results can be observed at both wind speeds (results from V = 7 and 10 m/s wind speed s were almost identical). The average and the standard deviation of the harmonic terms corresponding to Anemometer-1 units are larger than the ones corresponding to Anemometer-2 units, with the exception of the third harmonic term. The lower values of the harmonic terms different from the third one (n = 3) suggest a more accurate response of Anemometer-2 (that is, a less noisy signal). Also, the standard deviation of the third harmonic term corresponding to Anemometer-1 seems quite large in comparison to the other harmonic terms, revealing higher differences related to the rotor aerodynamics between different units than the ones shown by Anemometer-2 units.

Bearing in mind that the first and third harmonic terms, ω_1/ω_0 and ω_3/ω_0, respectively, reflect perturbations affecting the rotor's movement [23], different behavior is observed between Anemometer-1 and Anemometer-2 models. See in Figs. 7 and 8 the frequency histograms corresponding to these harmonic terms, calculated for both cup anemometer models. Analyzing the first harmonic term histograms (Fig. 7), differences between Anemometer-1 and Anemometer-2 arise immediately. In case of Anemometer-1 histogram the first harmonic exhibits a symmetrical Gaussian distribution, whereas Anemometer-2 units show a skewed right distribution. Also, the average value of the first harmonic term is higher for the Anemometer-1 units, which agrees with the information from Fig. 6.

In relation to the third harmonic term histograms, the distribution shown by Anemometer-1 has a larger variance (which is coherent with the information from Fig. 6, i.e., larger standard deviation), with even two peaks, one centered on ω_3/ω_0 = 0.013 and the other one centered on ω_3/ω_0 = 0.008. On the contrary, the histogram shown by Anemometer-2 units has a lower variance. These results point out the relevancy of future research on the harmonic terms statistics from large series of units. However, this research is out of the scope of the present work.

As said in the previous section, as the sampling period is normally composed by a number of complete turns of the rotor plus one not complete turn, some deviation may be introduced in the measurements. In order to evaluate this effect (i.e., not calculating the rotation speed based on complete turns of the rotor instead of counting number of pulses within a sampling period), the differences of the rotation speed measured as a data-logger does, $\bar{\omega}$ (see Eq. (13)), and the rotation speed calculated taking only into account complete turns of the rotor within the sampling period, ω_{ct}, have been calculated. In all cases (that is, for all 20 s datasets from Anemometer-1 and Anemometer-2 units calibrations), $\bar{\omega}$ and ω_{ct}, were calculated within sampling time frames of T_d = 1, 3, 5, 10 and 15 s. The error associated to the sampling in a frame was defined as $(\bar{\omega}-\omega_{ct})/\omega_{ct}$. The sampling frames were displaced, in steps of Δt = 0.0002 s, from the beginning of the dataset (t = 0 s) to the end of it (t = 20 s), in order to obtain the maximum values that characterize the error of the sampling period, T_d, for an individual anemometer at a specific wind speed:

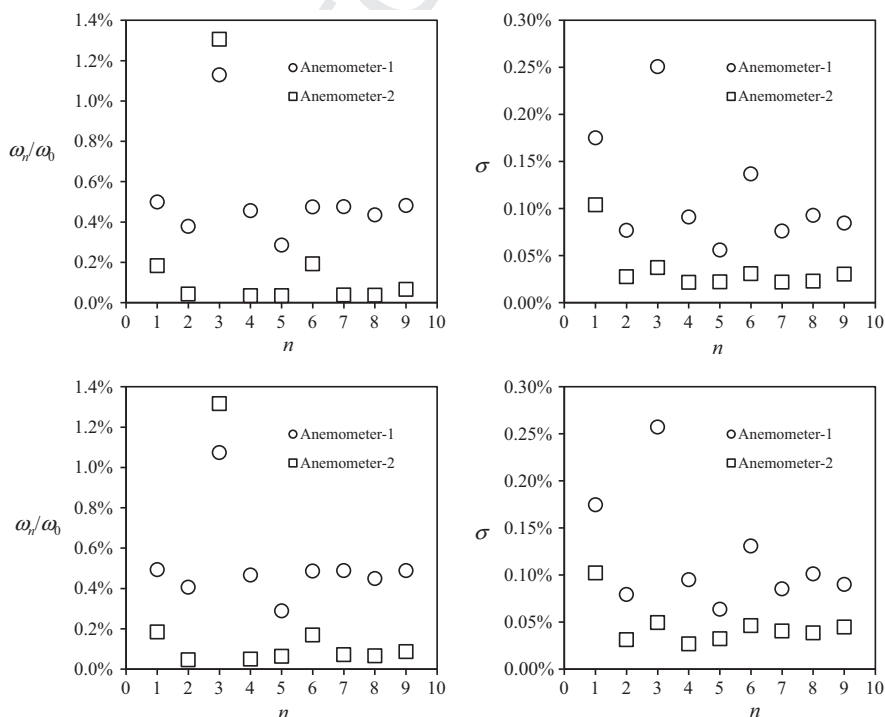$$\varepsilon_s = \left\| \frac{\bar{\omega} - \omega_{ct}}{\omega_{ct}} \right\|_{\max}. \tag{18}$$

Fig. 6. Average value, ω_n/ω_0, and standard deviation, σ, of the first nine harmonic terms calculated in relation to Anemometer-1 and Anemometer-2 units at V = 4 m/s (top) and 16 m/s (bottom) wind speeds.
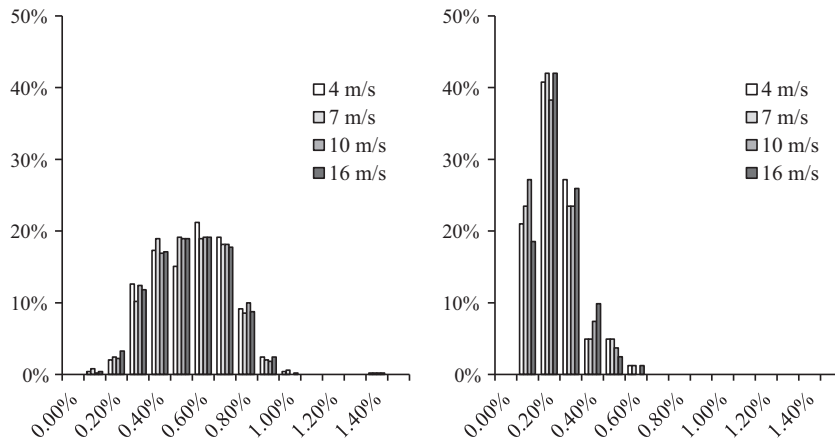
A. Martínez et al. / Measurement xxx (2016) xxx–xxx

Fig. 7. Frequency histograms of the first harmonic term, ω_1/ω_0, calculated on the Anemometer-1 (left) and Anemometer-2 (right) units studied in the present work.
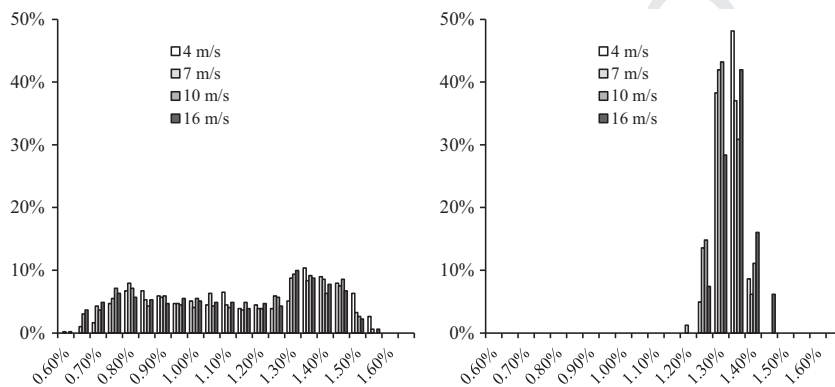

Fig. 8. Frequency histograms of the third harmonic term, ω_3/ω_0, calculated on the Anemometer-1 (left) and Anemometer-2 (right) units studied in the present work.

Using this procedure it is possible to get a value of the maximum possible sampling error for the analyzed unit, as a function of the wind speed and the sampling time.

In Fig. 9, the effect of the first harmonic term on the calculated error, ε^*, and the measured error, ε_s, due to the sampling period chosen (T_d = 1 s, in this case) at 4 m/s wind speed, are included for Anemometer 1 and Anemometer-2 units. Despite the high level of scatter shown by results (especially concerning ε_s), a linear behavior seems to be shown in the graphs in relation to both errors. In Fig. 10, the same results have been included increasing the sampling period to T_d = 10 s, the same linear behavior being

observed in relation to the calculated error, ε^*. However, the scatter showed by the measured error, ε_s, does not allow any conclusion regarding the possible linear effect of the first harmonic term, ω_1/ω_0, on it. In Fig. 11, the errors are shown taking a sampling period of T_d = 1 s, and at 16 m/s. The calculated error, ε^*, shows a linear pattern in relation to Anemometer-1 and Anemometer-2 units, whereas the measured error, ε_s, show a scattered pattern in both cases. Additionally, this last error seems to be focused on two different levels for Anemometer-1 units suggesting the same tendency shown in the histogram from Fig. 8.
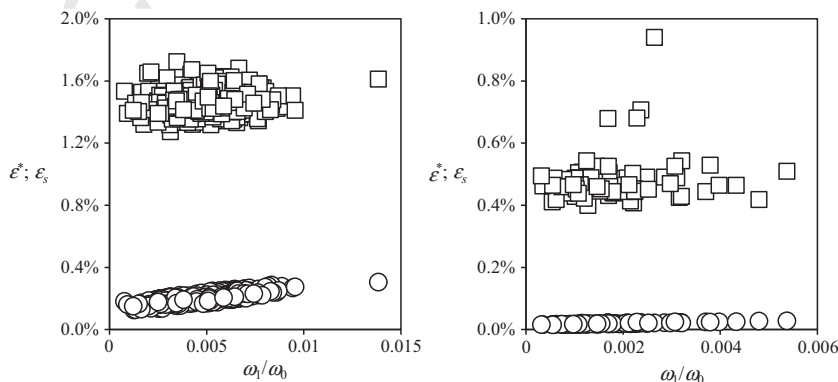

Fig. 9. Calculated error, ε^* (circles), and measured error, ε_s (squares), for sampling period T_d = 1 s, at 4 m/s wind speed, in relation to Anemometer 1 (left) and Anemometer-2 (right) units.
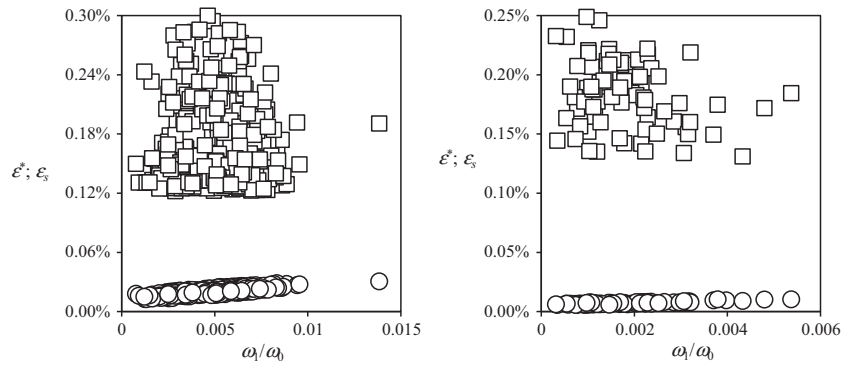
7

Fig. 10. Calculated error, ε^* (circles), and measured error, ε_s (squares), for sampling period T_d = 10 s, at 4 m/s wind speed, in relation to Anemometer 1 (left) and Anemometer-2 (right) units.
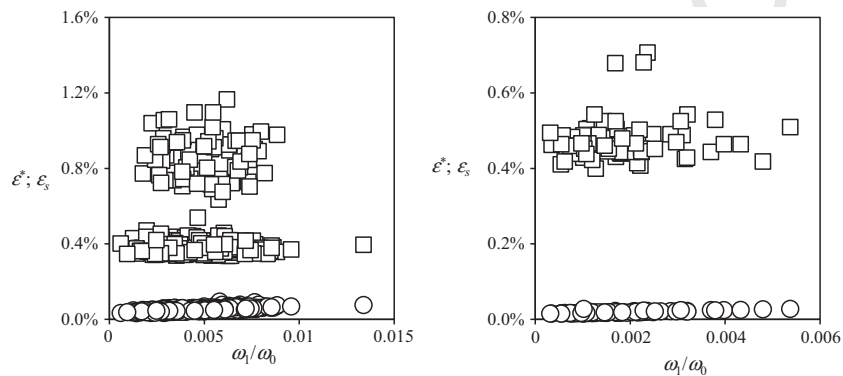

Fig. 11. Calculated error, ε^* (circles), and measured error, ε_s (squares), for sampling period T_d = 1 s, at 16 m/s wind speed, in relation to Anemometer 1 (left) and Anemometer-2 (right) units.

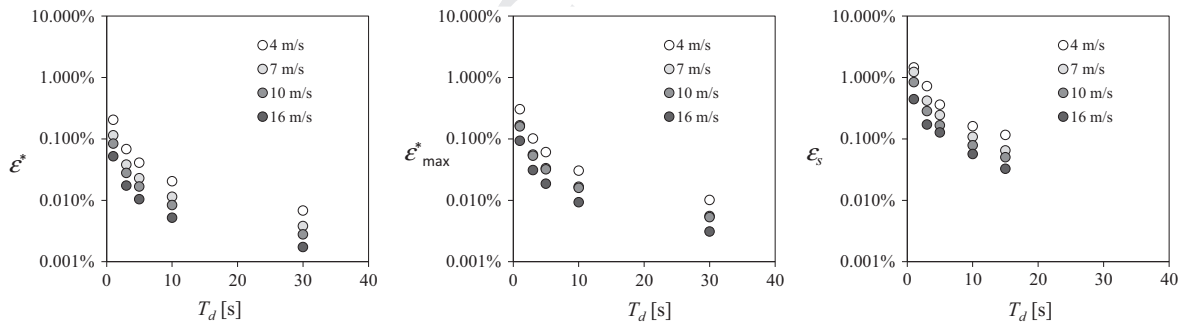**Fig. 12.** Anemometer-1 units: averaged and maximum errors based on the harmonic terms (ε^* and ε^*_{max}, calculated with Eq. (8)), as a function of the sampling period and for the studied wind speeds (left and middle graphs). The maximum sampling error, ε_s, found studying all units have been also added (right graph).

Fig. 13. Anemometer-2 units: averaged and maximum errors based on the harmonic terms (ε^* and ε^*_{max}, calculated with Eq. (8)), as a function of the sampling period and for the studied wind speeds (left and middle graphs). The maximum sampling error, ε_s, found studying all units have been also added (right graph).
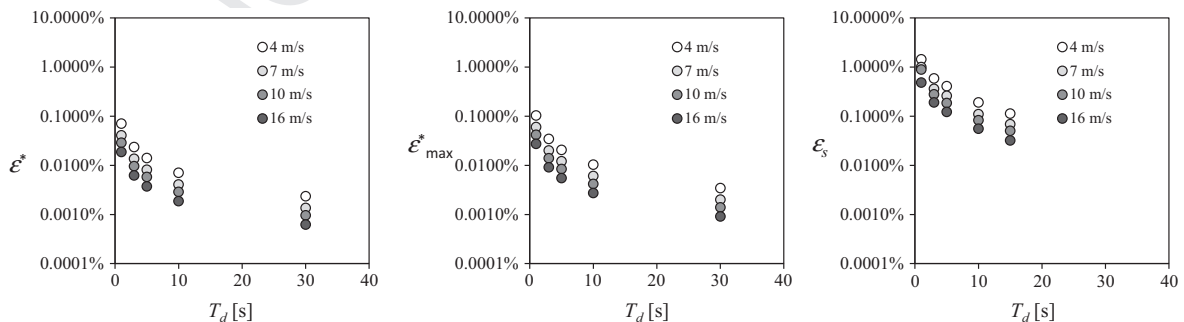
The measured errors, ε_s, shown in Figs. 9–11 are larger than the ones previously calculated in Section 2.1, based on the Thies 4.3303 cup anemometer signature ($\varepsilon_{s,max}$, see Table 2). The possible explanation of this lies on the uncertainties linked to the measurement process [30,13] which can reach values above 1%, as said in the first section of the present work. Nevertheless, it should also be fair to say that MEASNET procedures keep these uncertainties within strict limits [26,27].

In Figs. 12 and 13, the averaged and maximum calculated errors (ε^* and ε_{max}^*, see Eq. (8)) based on the harmonic terms derived from the testing data are respectively shown for Anemometer-1 and Anemometer-2 units. Anemometer-2 units show a slightly lower level of error when compared to Anemometer-1, on the other hand, the maximum error as a function of the sampling time is quite similar to the average error calculated upon all units. In these figures, the averaged values of these measurement errors, ε_s, have been included for Anemometer-1 and Anemometer-2 units, the results being similar between both models, and larger than the errors analytically calculated with Eq. (8). Nevertheless, it should be underlined that the errors linked to the sampling period (i.e., errors due to not taking complete turns of the rotor), measured and calculated in the present work seems to be reduced, as the maximum for the analyzed unit is around 1% for 1 s sampling period.

4. Conclusions

In the present work the deviation of the rotation speed measurements due to the sampling period chosen (as it normally includes one not complete turn of the rotor together with complete turns), has been demonstrated both analytically and experimentally, the experimental analysis being based on a large pool of measurements. This deviation is directly related to the error on the wind speed measurements through the anemometer transfer function (i.e., the calibration curve), which correlates the output frequency to the wind speed. The most significant conclusions derived from the present work are the following:

- The analytical results show a deviation mainly produced by the first harmonic term of the rotation speed of the anemometer. This fact was confirmed by the results extracted from the testing data.
- The deviation found seems not relevant if it is compared to other more significant sources of uncertainty, as stated in the first section of the present work. However, it can be easily excluded if the measurement process of the cup anemometer (together with the calibration) is based on complete turns of the rotor instead of a fixed sampling period.
- Some interesting results were found in relation to the rotation speed harmonic terms calculated from the large series of anemometers analyzed. Although much technical effort is still needed to understand the relationship between the anemometer fabrication processes and the distribution of the harmonic terms, it could be possible to implement simple and quick tests (short activation of the rotor while measuring the output signal) to start research campaigns inside the companies.

Acknowledgements

References

[1] S. Pindado, J. Cubas, F. Sorribes-Palmer, The cup Anemometer, a fundamental meteorological instrument for the wind energy industry. Research at the IDR/UPM Institute, Sensors 14 (2014) 21418–21452.
[2] A. Sanz-Andrés, S. Pindado, F. Sorribes, Mathematical analysis of the effect of the rotor geometry on cup anemometer response, Sci. World J. 2014 (2014) 1–23.
[3] J.C. Wyngaard, J.T. Bauman, R.A. Lynch, Cup anemometer dynamics, Flow: Meas. Control Sci. Ind. 1 (1974) 701–708.
[4] N.E. Busch, L. Kristensen, Cup Anemometer Overspeeding, J. Appl. Meteorol. 15 (1976) 1328–1332.
[5] P.A. Coppin, An examination of cup anemometer overspeeding, Meteorol. Rundsch. 35 (1982) 1–11.
[6] J.C. Wyngaard, Cup, propeller, vane, and sonic anemometers in turbulence research, Annu Rev. Fluid Mech. 13 (1981) 399–423.
[7] L. Makkonen, L. Helle, Calibration of anemometers—an uncertainty in wind energy resource assessment, in: Proceedings of the Fifth European Wind Energy Association Conference (EWEA), 1994, pp. 273–278.
[8] L. Makkonen, P. Lehtonen, L. Helle, Anemometry in icing conditions, J. Atmos. Ocean. Technol. 18 (2001) 1457–1469.
[9] L. Kristensen, O.F. Hansen, J. Højstrup, Sampling bias on cup anemometer mean winds, Wind Energy 6 (2003) 321–331.
[10] R.S. Hunter, The accuracy of cup anemometer calibration with particular regard to wind turbines, Wind Eng. 14 (1990) 32–43.
[11] R.S. Hunter, T.F. Pedersen, P. Dunbabin, I. Antoniou, S. Frandsen, H. Klug, A. Albers, W.K. Lee, European wind turbine testing procedure developments task 1: measurement method to verify wind turbine performance characteristics, Risø-R-1209(EN) (Roskilde, Denmark), 2001.
[12] R.S. Hunter, B.M. Petersen, T.F. Pedersen, H. Klug, N. van der Borg, N. Kelley, J.A. Dahlberg, Recommended practices for wind turbine testing and evaluation, in: R.S. Hunter (Ed.), 11-Wind speed measurement and use of cup anemometry, Paris, France, 2003.
[13] P.J. Eecen, M. De Noord, Uncertainties in cup anemometer calibrations Type A and Type B uncertainties, ECN-C-05-066, Petten, The Netherlands, 2005.
[14] T. Ohmae, T. Matsuda, K. Kamiyama, M. Tachikawa, A microprocessor-controlled high-accuracy wide-range speed regulator for motor drives, IEEE Trans. Ind. Electron. IE-29 (1982) 207–211.
[15] R. Bonert, Digital tachometer with fast dynamic response implemented by a microprocessor, IEEE Trans. Ind. Appl. IA-19 (1983) 1052–1056.
[16] R. Bonert, Design of a high performance digital tachometer with a microcontroller, IEEE Trans Instrum. 38 (1989) 1104–1108.
[17] E. Galván, A. Torralba, L.G. Franquelo, ASIC implementation of a digital tachometer with high precision in a wide speed range, IEEE Trans Ind. Electron. 43 (1996) 655–661.
[18] R.C. Kavanagh, An enhanced constant sample-time digital tachometer through oversampling, Trans. Inst. Meas. Control. 26 (2004) 83–98.
[19] K. Hachiya, T. Ohmae, Digital speed control system for a motor using two speed detection methods of an incremental encoder, in: 2007 European Conference on Power Electronics and Applications, Aalborg, Denmark: IEEE, 2007, pp. 1–10.
[20] Y. Li, F. Gu, G. Harris, A. Ball, N. Bennett, K. Travis, The measurement of instantaneous angular speed, Mech. Syst. Signal Process. 19 (2005) 786–805.
[21] S. Pindado, E. Vega, A. Martínez, E. Meseguer, S. Franchini, I. Pérez, Analysis of calibration results from cup and propeller anemometers. Influence on wind turbine Annual Energy Production (AEP) calculations, Wind Energy 14 (2011) 119–132.
[22] J.-Å. Dahlberg, T.F. Pedersen, P. Busche, ACCUWIND -Methods for Classification of Cup Anemometers, Risø-R-1555(EN), Roskilde, Denmark, 2006.
[23] S. Pindado, J. Cubas, F. Sorribes-Palmer, On the harmonic analysis of cup anemometer rotation speed: a principle to monitor performance and maintenance status of rotating meteorological sensors, Measurement (2015).
[24] E. Vega, S. Pindado, A. Martínez, E. Meseguer, L. García, Anomaly detection on cup anemometers, Meas. Sci. Technol. 25 (127002) (2014) 6.
[25] S. Pindado, J. Cubas, A. Sanz-Andrés, Aerodynamic analysis of cup anemometers performance. The stationary harmonic response, Sci. World J. 2013 (2013) 1–11.
[26] MEASNET, Cup anemometer calibration procedure, Version 1 (September 1997, updated 24/11/2008), Madrid, Spain, 1997.
[27] MEASNET, Anemometer calibration procedure, Version 2 (October 2009), Madrid, Spain, 2009.
[28] S. Pindado, J. Pérez, S. Avila-Sanchez, On cup anemometer rotor aerodynamics, Sensors 12 (2012) 6198–6217.
[29] S. Pindado, I. Pérez, M. Aguado, Fourier analysis of the aerodynamic behavior of cup anemometers, Meas. Sci. Technol. 24 (065802) (2013) 9.
[30] R.V. Coquilla, J. Obermeier, B.R. White, Calibration procedures and uncertainty in wind power anemometers, Wind Eng. 31 (2007) 303–316.